10.1109/ULTSYM.2011.0232

Probing microbubble adhesion using secondary acoustic radiation force

T.J.A. Kokhuis[1,7*], V. Garbin[2], K. Kooiman[1], B.A. Naaijkens[4,7], L.J.M. Juffermans[5,7], O. Kamp[6,7], M. Versluis[3], A.F.W. van der Steen[1,7] and N. de Jong[1,3,7]

[1] Biomedical Engineering, Thorax Center, Erasmus MC, Rotterdam, the Netherlands
[2] Department of Chemical and Biomolecular Engineering, University of Pennsylvania, Philadelphia, USA
[3] Physics of Fluids group, University of Twente, Enschede, the Netherlands
[4] Department of Pathology, VU University Medical Center, Amsterdam, the Netherlands
[5] Department of Physiology, VU University Medical Center, Amsterdam, the Netherlands
[6] Department of Cardiology, VU University Medical Center, Amsterdam, the Netherlands
[7] Interuniversity Cardiology Institute of the Netherlands, Utrecht, the Netherlands

Abstract – **In this study we investigated the translational dynamics of mutually attracting targeted microbubbles during and after ultrasound (US) insonification in more detail and show this mutual attraction can be used to determine the binding force. In general, similar sized microbubbles are known to attract each other during US application as a result of an acoustic radiation force leading to clustering and coalescence. Targeted microbubbles, however, move back to their initial position after US is turned off, implying the presence of an elastic restoring force, which in turn opposes the net pulling force. From the recoiling curves, a value for the effective spring constant *k* could be obtained, which was of the order of 2.4 mN/m. For higher acoustic pressures the pulling force exceeded the binding force and the bubbles detached. A threshold force for detachment was calculated with the obtained value of the spring constant. For biotinylated microbubbles (R=2-2.5 µm) targeted to a NeutrAvidin coated surface, the threshold force was between 0.9 nN and 2.0 nN. We also show that the translational dynamics of targeted microbubbles during US application can be modelled accurately using a hydrodynamic model [1], including a value for the spring constant *k* of the very same order as derived experimentally.**

Keywords – targeted microbubbles, acoustic radiation force, binding force, translational dynamics, detachment

I INTRODUCTION

Targeted microbubbles have the ability to specifically bind to pathological targets on the vascular endothelium. In combination with their echogenic properties they facilitate targeted contrast-enhancement during ultrasound (US) insonification, also called molecular ultrasound imaging [2]. However, in a parallel plate flow cell study Schmidt *et al.* (2008) observed detachment and aggregation of biotinylated microbubbles targeted to a NeutrAvidin coated surface during insonification [3], indicating molecular ultrasound imaging is not always straightforward. The effects observed were ascribed to the mutual interaction between the microbubbles, termed secondary acoustic radiation force or secondary Bjerknes force [4,5]. The instantaneous secondary acoustic radiation force exerted on the bubble is alternating between attractive and repulsive. However, when averaged over one cycle, there is a net force which is attractive for two bubbles oscillating in phase and repulsive for two bubbles oscillating out of phase [5].

In order to maximally benefit from the potentials of molecular ultrasound imaging a thorough understanding of the effect of secondary acoustic radiation force on the adhesion of targeted microbubbles is essential. On the other hand, if secondary acoustic radiation force can detach targeted microbubbles, it can have potential for assessing the binding force of targeted bubbles, an important parameter that determines the adherence efficiency of the bubbles when subjected to shear flow *in vivo*. In this study we used the ultra high-speed Brandaris128 camera [6] to investigate the dynamics of targeted microbubbles under influence of secondary acoustic radiation forces in more detail. The objective was twofold. First, to understand the translational dynamics of targeted microbubbles at the level of a hydrodynamic point-force model [1], using input parameters derived from experiment. Second, to estimate from the experimental data the bubble binding force from the point of detachment as a result of the mutual attraction between the targeted microbubbles.

II MATERIALS AND METHODS

A. *Preparation of microbubbles*

Biotinylated microbubbles with a perfluorobutane (C_4F_{10}) gas core were made by sonication, as described in [7]. The coating was composed of DSPC (59.4 mol %), PEG-40 stearate (35.7 mol%), DSPE-PEG(2000) (4.1 mol %) and DSPE-PEG(2000)-biotin (0.8 mol %).

B. *High speed imaging of targeted bubbles*

A thin polystyrene membrane coated with NeutrAvidin served as target surface. Biotinylated microbubbles were allowed to interact with the target surface by flotation for 10 minutes. After that the membrane was mounted on top of a water tank with the targeted bubbles on top. Microbubbles were insonified at varying peak negative pressures (P_= 0-330

kPa) with 20 cycles at 2.25 MHz. The bubbles were imaged with a customized microscope and images were relayed to the ultra fast-framing Brandaris128 camera [6].

C. Numerical simulations

Hydrodynamic model during US insonification

A hydrodynamic point-force model for two pulsating bubbles targeted to a wall was proposed in [1] to model the microbubble translational dynamics during US insonification. Here, the restoring force term is replaced with a Hookean spring model, including an effective spring constant *k*. We will briefly recall the forces included in the model. For a more detailed description of the model, the reader is referred to [1].

The total force balance on a bubble 1, due to a pulsating bubble 2, along the centre-centre line is given by:

$$\vec{F}_R + \vec{F}_{AM} + \vec{F}_{QS} + \vec{F}_H + \vec{F}_K = 0 \quad (1)$$

The driving force is the secondary acoustic radiation force $\vec{F}_R$ which is given by:

$$\vec{F}_R = -(1+\beta)\rho\frac{4}{3}\pi R_1^3\left(\frac{\ddot{R}_2 R_2^2 + 2R_2\dot{R}_2^2}{d^2}\right) \quad (2)$$

with ρ the density of the surrounding fluid, d the centre-centre distance, R_1 the radius of bubble 1, R_2 the radius of bubble 2 and the overdots the corresponding time derivatives. The factor *β* represents the reflection coefficient of the polystyrene wall and accounts for the increase of the pressure gradient experienced by the bubble due to wall reflections.

$\vec{F}_{QS}$ accounts for the quasi-steady component of the drag force, and is given by:

$$\vec{F}_{QS} = -6\pi\mu R_1\vec{U}_1 \quad (3)$$

with μ the dynamic viscosity of the surrounding fluid and $\vec{U}_1$ the velocity of the bubble relative to the fluid.

$\vec{F}_{AM}$ is the added mass force given by:

$$\vec{F}_{AM} = -\frac{1}{2}\rho\left(V_1\frac{\partial\vec{U}_1}{\partial t} + \vec{U}_1\frac{\partial V_1}{\partial t}\right) \quad (4)$$

with V_1 the volume of bubble 1.

$\vec{F}_H$ denotes the history force, accounting for unsteady viscous dissipation, and is given by [1,8]:

$$\vec{F}_H = -6\pi\rho\sqrt{\frac{\nu}{\pi}}\int_0^t \frac{d\tau}{\sqrt{\int_\tau^t R_1(s)^{-2}ds}}\frac{d(R_1\vec{U}_1)}{dt} \quad (5)$$

with ν the kinematic viscosity of the surrounding fluid.

And finally, a restoring force, responsible for the microbubble recoiling, is included:

$$\vec{F}_K = -k\vec{x}_1 \quad (6)$$

with *k* the effective spring constant and $\vec{x}_1$ the displacement of bubble 1 with respect to its initial position. The forces on bubble 2 due to a pulsating bubble 1 can be obtained by exchanging the subscripts above from 1 to 2. The experimental radius-time curves of bubble 1 and 2 and the corresponding first and second derivatives were used as input for the numerical simulations, following a procedure detailed in [1]. The two coupled second-order differential equations were solved numerically.

Hydrodynamic model after US insonification

After US insonification the radial pulsations cease and contributions from the secondary acoustic radiation force, history force and second term of the added mass force can be discarded from the force balance. The restoring force, which is responsible for pulling the microbubbles back to their original position, acts against the added mass force and the quasi-steady drag force. The force balance on a bubble therefore reduces to:

$$\vec{F}_{AM} + \vec{F}_{QS} + \vec{F}_K = 0 \quad (7)$$

The resulting second-order (uncoupled) differential equation was solved numerically for each bubble.

III Results

A. Translational dynamics during US insonification

At relatively low acoustic pressures, targeted microbubbles were observed to exhibit "spring-like" behaviour. Microbubbles moved towards each other during US insonification but were observed to have recoiled back to their initial position by the start of the next experiment, 80 ms after the US was turned off. After insonification at higher acoustic pressures, the microbubbles were observed to have moved substantially in the direction of the neigbouring bubble by the start of the next experiment. The bottom panel of Fig. 1 shows the evolution of

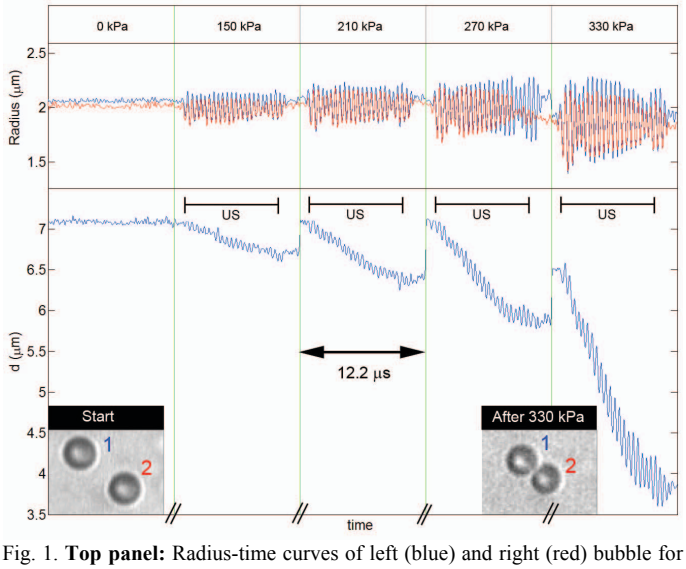

Fig. 1. **Top panel:** Radius-time curves of left (blue) and right (red) bubble for various pressures (0-330 kPa). **Bottom panel**: Centre-centre distance curve d(μm). The radius of both bubbles was 2 μm.

the centre-centre distance, d (μm), between the two microbubbles during 5 subsequent experiments with increasing pressures (P_= 0-330 kPa). The top panel shows the corresponding radius-time curves for the left bubble (blue) and the right bubble (red) and the green lines indicate the position of the 80 ms time interval between subsequent experiments. In the first experiment, no US was applied. During the 150 kPa and 210 kPa experiments, the centre-centre distance was observed to decrease by 500 nm and 800 nm, respectively. However, in both cases it had again recovered to the initial value of 7.1 μm by the start of the next experiment 80 ms afterwards. On the other hand, by the start of the 330 kPa experiment a 600 nm decrease of the centre-centre distance was observed. Both bubbles were detached from their initial binding position, implying the adhesion of both bubbles broke during insonification with 270 kPa. Additional insonification with 330 kPa resulted in clustering of the bubbles (see right inset; left inset shows initial situation).

B. Translational dynamics after US insonification

To study the apparent recoiling of the microbubbles after US insonification (i.e. in the undriven case), microbubbles were insonified and this time imaged at a relatively low frame rate near 1 Mfps. The result of 6 subsequent experiments (P_=0-300 kPa), is shown in Fig. 2. Each individual experiment (start/end indicated again by the green vertical lines) covered a time window of ~ 110 μs. Microbubbles were insonified during the first eight frames of each movie, indicated by the orange transparent window. The remaining part of the movies captured the recoiling afterwards. As observed before, the centre-centre distance decreased during insonification and increased for increasing acoustic pressures. When the US was turned off, the centre-centre distance reached a minimum value (10.3 μm, 10.1 μm and 9.2 μm for the 180 kPa, 240 kPa and 300 kPa experiments respectively), after which the microbubbles moved back in the opposite direction. After insonification with 180 kPa and 240 kPa, the centre-centre distance was observed to recover to the initial value of 10.8 μm within 80 μs. However, insonification with 300 kPa resulted detachment of the bubbles from their initial binding position; the distance in between was observed to equilibrate at the new value of 10.2 μm afterwards.

C. Effective spring constant and threshold force

The results shown in Fig. 1 and Fig. 2 clearly indicate the presence of restoring forces, pulling the microbubbles back to their initial position after the US is turned off. To quantify the value of the corresponding equivalent spring constant k, the experimental recoiling curves of figure 2 were fitted with the hydrodynamic model after US (equation (7)). Using least squares fitting, a value of k = 2.4 mN/m was obtained (R^2 = 0.98). We assume a microbubble will start to detach when the internal restoring force (which opposes the attractive pulling force) overcomes the adhesion force of the microbubble to the substrate. With the obtained value of k, we can now estimate the internal restoring force (equation (6)) the adhesive belt of a microbubble was subjected to. Fig. 2 shows that the distance between the two bubbles still recovers to the initial value of 10.8 μm after a centre-centre decrease of 0.7μm (i.e. 0.35 μm of translation per bubble). However, after a centre-centre decrease of 1.6 μm (i.e. 0.8 μm of translation per bubble) the distance did not recover to the initial value. The threshold force at which these microbubbles started to detach from the surface should therefore be between 0.9 nN and 2 nN.

D. Numerical simulation during US

Fig. 3 shows the comparison between the evolution of the centre-centre distance, d(μm), between two bubbles (insonified with 20 cycles at 210 kPa) obtained experimentally and as predicted by the hydrodynamic point-force model of equation (1). By using a value for the equivalent spring constant of k = 6 mN/m (red curve), i.e. of the very same order as obtained experimentally from a different set of bubbles, excellent agreement with the experimental curve (blue) is obtained. The final separation distance is predicted well by the model, including the start of the recoil. On the other hand, neglecting the restoring force (k = 0 mN/m, black curve) leads to a dramatic overestimation of the decrease in the separation distance.

IV DISCUSSION

Secondary acoustic radiation force can detach targeted microbubbles from a surface. Insonifying the bubbles repeatedly resulted in the formation of stable clusters (Fig. 1) that remained bound to the substrate after the experiment, instead of floating out of the optical focus due to buoyancy. This suggests that targeted bubbles are able to reattach to the substrate after being locally detached from their initial binding position.

In this study we investigated the recoil of targeted microbubbles after US insonification in more detail and determined a value for the equivalent spring constant k (2.4 mN/m). The experimentally obtained recoil curves (Fig. 2) were fitted to the hydrodynamic model for translation of targeted microbubbles as proposed in [1], in which we substituted the restoring term with the equation of a Hookean spring ($F = -kx$). The obtained value of k depends on the drag terms included in the model. As already mentioned in reference [1], possible effects of sliding friction between the translating bubble and the wall and increased viscous effects due to the presence of the

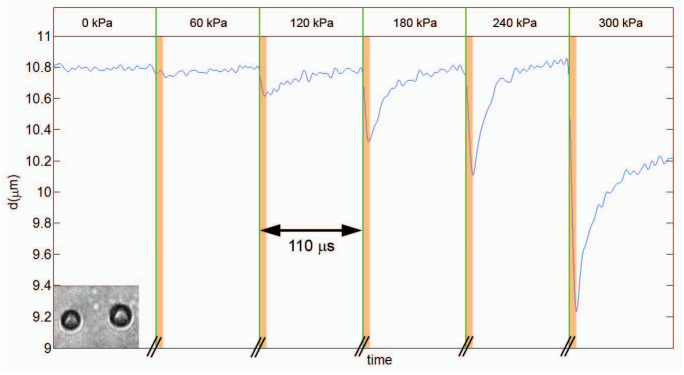

Fig. 2. Evolution of the centre-centre distance (d(μm)) between the two microbubbles shown in the inset, during (transparent orange bar) and after insonification, for different pressures (0-300 kPa). The radius of the left and right bubble was 2.2 μm and 2.4 μm respectively.

boundary layer are not included in the model. From our excellent agreement between theory and experiment in the US-driven and undriven case, including a similar value of the effective spring constant k in both cases, we can actually deduce that the effects of friction and the boundary layer are not prominent in our case. The inclusion of more drag terms in our model would effectively result in an increased value of the obtained effective spring constant k in order to fit the experimental data in the undriven case (after US). However, inclusion of more drag terms, as well as an increased value of the effective spring constant k will worsen the fit in the driven case (during US) at the same time, justifying *a posteriori* the neglect of additional drag terms. Moreover, calculations performed in [9] on the friction between a translating bubble subjected to primary acoustic radiation force, in contact with a wall, revealed the friction term to be an order of magnitude smaller than the other drag forces acting on the bubble, supporting our assumptions above.

The force needed to detach bubbles from the substrate was estimated to be of the order of 1 nN. Using micropipette aspiration, Kim *et al.* studied the adhesion force between an avidin coated glass bead and a large bubble (~30 µm in diameter) for a variety of molar fractions of biotin [10]. For the molar fraction used in our study (i.e. 0.8 %) the mean detachment force was about 20 nN. From microscopic observations, the contact area of their system was estimated to be 10 µm^2. The contact area A involved in the binding of our microbubbles can be approximated by $A = 2\pi Rh$, where h represents the maximum distance where bonds can be formed. If we take $h \sim 16$ nm, which corresponds to the fully extended length of the PEG2000 spacer [11], and R = 2 µm, the estimated contact area is ~ 0.20 µm^2. If we assume the adhesion force to be proportional to the contact area, we would expect to measure a binding force that is about 50 times smaller, i.e. ~ 0.4 nN, which is in reasonable agreement with the values reported here.

The origin of the apparent restoring force could not be distilled from our current dataset. To elucidate its physical origin, the targeted bubbles will be imaged using an orthogonal optical setup, facilitating simultaneous top and side view imaging [12]. Even though no significant bubble deformation was observed from the top view during all of our experiments, a side view image may reveal a deformation that would assist the recoil phenomenon. Another possibility is that the microbubbles form elongated tethers or wrinkles [13] during US insonification, similar to what has been observed in neutrophil rolling in shear flow [14]. Although at a different time scale as the recoiling reported here, these elongated tethers were observed to pull back a neutrophil after the shear flow was reduced [15].

In conclusion, secondary acoustic radiation force shows potential to quantify the adhesion force of targeted microbubbles. Moreover, we have shown that the translational dynamics of a targeted microbubble subjected to secondary acoustic radiation force can be modeled with accuracy using a hydrodynamic point-force model, including a restoring force. Understanding the behaviour of targeted microbubbles during insonification is crucial for future advances in the field of molecular imaging.

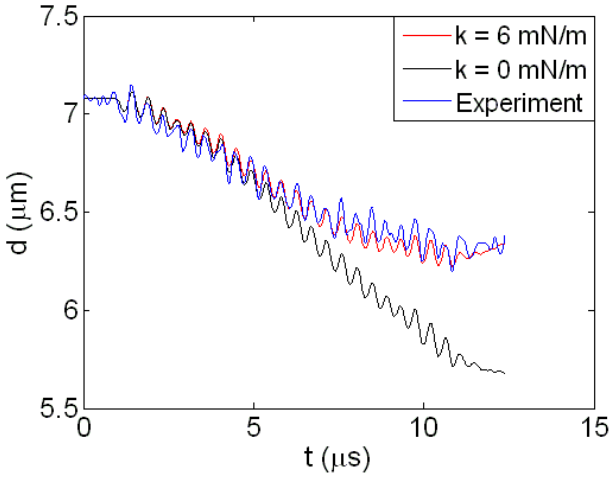

Fig. 3 Comparison between experimentally obtained (blue) and simulated (k = 6 mN/m, red) and k= 0 mN/m (black)) evolution of the centre-centre distance (d (µm)) between two microbubbles during 20 cycles of US at 210 kPa.

ACKNOWLEDGMENT

This work was financially supported by the Dutch Technology Foundation (STW).

REFERENCES

[1] Garbin, V. *et al.* Unbinding of targeted ultrasound contrast agent microbubbles by secondary acoustic forces. *Phys Med Biol* **56**, 6161-6177, 2011.

[2] Deshpande, N., Needles, A. & Willmann, J. K. Molecular ultrasound imaging: current status and future directions. *Clin Radiol* **65**, 567-581, 2010.

[3] Schmidt, B. J., Sousa, I., van Beek, A. A. & Bohmer, M. R. Adhesion and ultrasound-induced delivery from monodisperse microbubbles in a parallel plate flow cell. *J Control Release* **131**, 19-26, 2008.

[4] V.F.K. Bjerknes. Fields of force. Colombia University Press, 1906.

[5] Leighton, T. G., The Acoustic Bubble, Academic Press, 1994.

[6] Chin, C. T. *et al.* Brandaris 128: A digital 25 million frames per second camera with 128 highly sensitive frames. *Rev Sci Instrum* **74**, 5026-5034, 2003.

[7] Klibanov, A. L. *et al.* Detection of individual microbubbles of ultrasound contrast agents: imaging of free-floating and targeted bubbles. *Invest Radiol* **39**, 187-195, 2004.

[8] Garbin, V. *et al.* History force on coated microbubbles propelled by ultrasound. *Physics of Fluids* **21**, -, 2009.

[9] Dayton, P. A., Allen, J. S. & Ferrara, K. W. The magnitude of radiation force on ultrasound contrast agents. *J Acoust Soc Am*, **112**, 2183-2192, 2002.

[10] Kim, D. H., Klibanov, A. L. & Needham, D. The influence of tiered layers of surface-grafted poly(ethylene glycol) on receptor-ligand-mediated adhesion between phospholipid monolayer-stabilized microbubbles and coated glass beads. *Langmuir* **16**, 2808-2817, 2000.

[11] Moore, N. W. & Kuhl, T. L. The role of flexible tethers in multiple ligand-receptor bond formation between curved surfaces. *Biophys J* **91**, 1675-1687, 2006.

[12] Vos, H. J., Dollet, B., Bosch, J. G., Versluis, M. & de Jong, N. Nonspherical vibrations of microbubbles in contact with a wall: a pilot study at low mechanical index. *Ultrasound Med Biol* **34**, 685-688, 2008.

[13] Rychak, J. J., Lindner, J. R., Ley, K. & Klibanov, A. L. Deformable gas-filled microbubbles targeted to P-selectin. *J Control Release* **114**, 288-299, 2006.

[14] Park, E. Y. *et al.* Comparison of PSGL-1 microbead and neutrophil rolling: microvillus elongation stabilizes P-selectin bond clusters. *Biophys J* **82**, 1835-1847, 2002.

[15] Springer, T. A. & Chen, S. Q. An automatic braking system that stabilizes leukocyte rolling by an increase in selectin bond number with shear. *Journal of Cell Biology* **144**, 185-200, 1999.